J Atmos Chem (2008) 60:51–70
DOI 10.1007/s10874-008-9108-z

Novel measurements of atmospheric iodine species by resonance fluorescence

Catherine S. E. Bale · Trevor Ingham · Roisin Commane · Dwayne E. Heard · William J. Bloss

Received: 20 March 2008 / Accepted: 22 August 2008 / Published online: 11 September 2008

Abstract A field instrument has been developed for the purpose of measuring gas-phase atmospheric iodine species in the marine boundary layer. Vacuum UV resonance-fluorescence (RF), generated using a microwave discharge lamp, is employed to detect atomic iodine via the ($5p^4 6s$)–($5p^5$) transitions around 178–184 nm. The system can be operated in two modes; either to directly measure ambient iodine atoms, or to measure the total photolabile iodine loading of ambient air, through broadband visible photolysis of photolabile iodine-containing species, with subsequent RF detection of the iodine atoms released. In both cases the instrument allows for the in situ measurement of the species detected, which is advantageous for gathering information concerning their local sources and distribution. The instrument is calibrated through generation of a known concentration of iodine atoms from the photolysis of I_2 using a mercury pen-ray lamp. The instrument was deployed for the first time in August 2007 at Mace Head on the west coast of Ireland; initial results from this field trial are presented. Ambient iodine atoms were measured at levels up to 22±4.8 ppt during the day, coinciding with the lowest tides, when *Laminaria* seaweed beds were exposed. The total photolabile iodine loading was also measured during several night-time and day-time periods and was found to correlate inversely with tidal height. Inferred I_2 concentrations based on these measurements indicate levels of several hundred ppt at the Mace Head site. These measurements represent the first direct observations of ambient iodine atoms and measurement of total photolabile iodine in the atmosphere.

Keywords Iodine · Iodine monoxide · Mace head · Marine boundary layer · Resonance-fluorescence

C. S. E. Bale · T. Ingham · R. Commane · D. E. Heard
School of Chemistry, University of Leeds, Woodhouse Lane, Leeds LS2 9JT, UK

W. J. Bloss (✉)
School of Geography, Earth and Environmental Sciences, University of Birmingham, Edgbaston, Birmingham B15 2TT, UK
e-mail: w.j.bloss@bham.ac.uk

1 Introduction

The potential role of iodine species in the atmosphere has been considered for a number of years (e.g. Chameides and Davis 1980; Solomon et al. 1994). More recently, iodine species have been shown to affect the chemistry of the coastal marine boundary layer (MBL, e.g. Platt and Hönninger 2003; Carpenter 2003; von Glasow and Crutzen 2007), and have been measured in the polar boundary layer (Saiz-Lopez et al. 2007). In the marine environment, molecular iodine and alkyl iodides such as CH_3I and CH_2I_2 are emitted by micro and macro algae and undergo photolysis on timescales of seconds (I_2) to days (CH_3I) releasing their constituent iodine atoms, which then react with ozone, forming the iodine monoxide radical (IO).

$$I_2, RI \xrightarrow{h\nu} I \tag{1}$$

where R=CH_3, CH_2I, C_2H_5 etc.

$$I + O_3 \rightarrow IO + O_2 \tag{2}$$

IO is known to react with itself, HO_2 and NO_2 in cycles which may catalytically destroy tropospheric ozone (Chameides and Davis 1980; Vogt et al. 1999). As a result of such reactions, the OH:HO_2 and NO:NO_2 ratios may also be altered, which will in turn affect the oxidative capacity of the atmosphere (Bloss et al. 2005). It has also been suggested that the IO radical can polymerise via OIO/I_2O_2 to form larger condensable I_xO_y molecules, leading to aerosol growth and/or new particle formation, with potential implications for MBL cloud condensation nuclei abundance and hence radiative balance (O'Dowd et al. 2002).

Field measurements of species such as I_2, IO, and the alkyl iodides (CH_3I, CH_2I_2 etc.), have been made previously in the marine boundary layer: I_2 has been measured using long-pass differential optical absorption spectroscopy (DOAS; Saiz-Lopez and Plane 2004; Peters et al. 2005); however, this technique is associated with significant spatial and temporal averaging. IO and OIO have also been measured at various coastal sites using DOAS (e.g. Alicke et al. 1999; Saiz-Lopez et al. 2004). An issue for interpretation of DOAS observations, particularly at coastal sites such as Mace Head, has been the spatial distribution of iodine species: the DOAS beam path (usually several kilometres in length) may encompass both the intertidal zone and the open ocean, which can lead to ambiguity in the identification of the source of the iodine species (O'Dowd and Hoffmann 2005). Recently, new point measurement/in situ methods have been developed to measure OIO and I_2, via broadband cavity ringdown spectroscopy (Bitter et al. 2005) and IO, via laser-induced fluorescence (Whalley et al. 2007), however there has, as yet, been no direct (or indirect) atmospheric observations of atomic iodine, or the total photolabile iodine content.

The technique of resonance fluorescence (RF) for the detection of atomic iodine has been widely applied in laboratory experiments (e.g. Plane and Husain 1986; Ingham et al. 2000; Gross et al. 2000), but has not previously been applied in the form of a field measurement instrument. For laboratory experiments, achieving a high sensitivity, and therefore, low limit of detection, may not be as critical as for field measurements, and the concentrations sampled are in general several orders of magnitude larger (10^9–10^{12} cf. 10^7–10^8 atom cm^{-3}). Typically the limit of detection for laboratory instruments is of the order 10^9–10^{10} atom cm^{-3} or higher, raising challenges for field measurements; however the RF technique exhibits several advantages that make it an excellent choice for application as a

field instrument: high sensitivity, selectivity, low power consumption and potential for the components to be made lightweight and portable.

Atomic resonance fluorescence has been utilized for the detection of the other halogen species in the atmosphere, particularly the polar stratosphere. Anderson and co-workers developed a balloon-borne resonance-fluorescence instrument for the detection of ClO (by titration with NO and subsequent RF detection of the Cl atoms) in the stratosphere (Anderson et al. 1977, 1980). A similar instrument was also developed for the ER-2 aircraft to monitor stratospheric chlorine species (Brune et al. 1988, 1989a), with limits of detection better than 1 pptv. Subsequent developments allowed the detection of Cl_2O_2, via thermal decomposition followed by ClO titration with NO (Stimpfle et al. 2004). The chemical-conversion resonance-fluorescence (CCRF) technique has also been used for measurement of stratospheric BrO (Brune et al. 1989b) and more recently has been employed to detect ClO, Cl_2O_2 and BrO on the M55-Geophysica (von Hobe et al. 2005, 2006).

2 Instrument

The resonance lines of atomic iodine fall in the vacuum ultraviolet wavelengths in the range 170 – 190 nm. The two most important transitions are the $(5p^4\ 6s)\ ^2P_{3/2}$–$(5p^5)\ ^2P_{3/2}$ at λ=178.3 nm, and the spin-forbidden (and, therefore, 15–20 times weaker) $(5p^4\ 6s)\ ^4P_{5/2}$–$(5p^5)\ ^2P_{3/2}$ transition at λ=183.0 nm (Brewer and Tellinghuisen 1971). Absorption by molecular iodine, I_2, of light in the region between 180 and 200 nm through the highly structured (D←X) system will lead to population of the I_2 D $^1\Sigma_u^+$ state which fluoresces in the range 200–500 nm (O'Grady et al. 1982). As the photomultiplier used in this instrument detects radiation up to around 320 nm, a proportion of any I_2 fluorescence will be detected; any I_2 present therefore leads to an interference in the I-atom fluorescence signal but, as will be described later, this can be taken into account during calibration, and the sensitivity towards I_2 may be used advantageously. The instrument response to I_2 is, however, typically three orders of magnitude lower than that towards atomic iodine.

The instrument comprises a microwave discharge lamp and collimating optics to supply the excitation radiation, a fluorescence cell, detection optics, a photon counting module, data acquisition system and a separate calibration unit. Figure 1 shows a schematic diagram of the fluorescence cell setup.

2.1 Excitation radiation

Continuous-wave excitation radiation was generated in a Pyrex lamp using a microwave discharge to dissociate I_2 and produce excited I atoms. A small flow (10 sccm) of high purity helium (CP grade, >99.999% purity, BOC) regulated with a mass flow controller was continuously drawn through the lamp by a rotary vane vacuum pump. A small amount of I_2 vapour is entrained into the helium flow via a needle valve from a finger trap containing a few crystals of iodine. The pressure in the lamp was held at around 1 Torr and monitored with a 10 Torr capacitance manometer. The lamp is sealed with an MgF_2 window to allow transmission of the vacuum-UV radiation. The microwave discharge plasma is produced using an Evenson-type cavity supplied with 60 W of power (EMS Microtron 200). The lamp was kept clean from impurities by filling to above ambient pressure with helium when not in use. Periodically the lamp was washed with water to remove build-up of iodine on the inside surfaces, particularly on the exit window. Once the radiation has exited the lamp it was collimated using an MgF_2 plano-convex lens (Crystran Ltd.) and several baffles

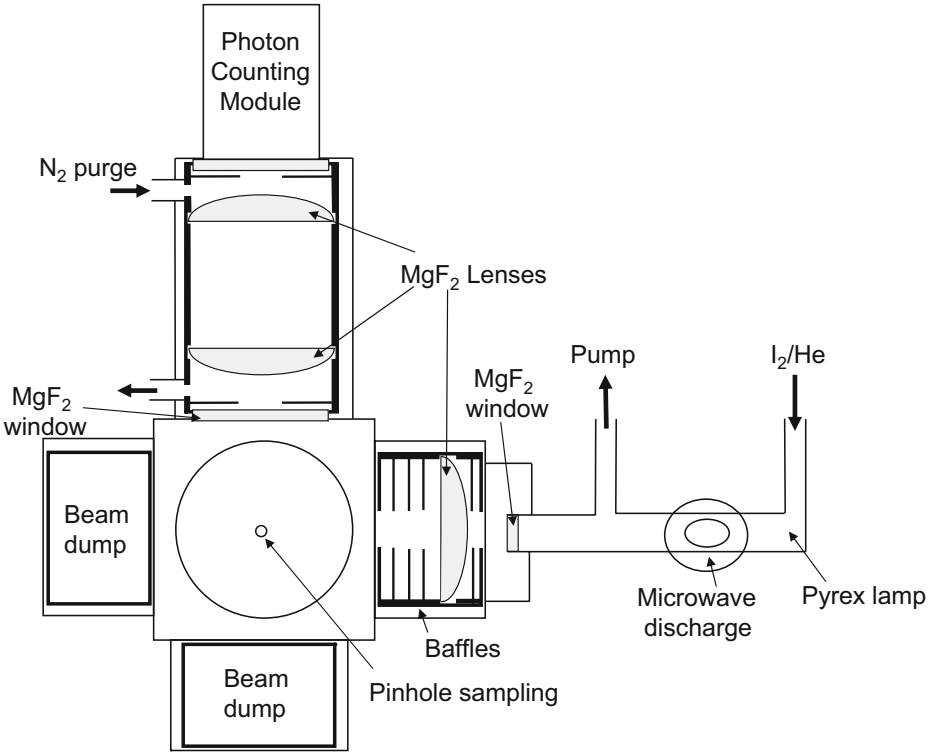

Fig. 1 Schematic diagram (plan view) of the RF instrument for the detection of atomic iodine. The main cell is constructed from a matt black anodised aluminium block. MgF_2 windows and lenses are used to allow transmission of the vacuum ultraviolet light. The pinhole is conically shaped with an aperture diameter of 0.8 mm. The lower face of the cell (not shown) houses connections to the pump, throttle valve and pressure gauge

(aperture diameter of 5 mm) before entering the fluorescence cell. Beam dumps were mounted within the cell opposite, and orthogonal to, the resonance lamp, to absorb scattered light and reduce the background signal (hence improving the limit of detection).

2.2 Fluorescence cell

The cell itself is an aluminium cube (65×65×65 mm), with 25 mm diameter holes bored through each face, anodised matt black to reduce scattering of light from the walls. The air sample is drawn through the cell at a rate of 5.6 slm through a conical pinhole (aperture diameter=0.8 mm), using a throttled rotary vane vacuum pump. Experimental tests revealed that the lowest cell pressure achievable with this setup (around 20 Torr using a 0.8 mm pinhole) gave the optimum sensitivity towards iodine atoms. Collisional quenching will increase with cell pressure, but will be balanced by increased total number density (as there is no time-resolved aspect to the fluorescence collection in this system). At significantly higher pressures, the increased transit time experienced by the atoms may allow chemical losses to become significant. The presence of a higher number density of O_2 and other molecules will also lead to increased scattering of the excitation light (raising the limit of detection) and absorption of the fluorescence light. Different sized pinhole apertures were tested (0.4–0.8 mm), in order to attain lower pressures in the cell. However, the sensitivity

was found to be best with a 0.8 mm diameter nozzle—likely to be a consequence of the optimum overlap of the expansion of the sampled gas within the cell, the excitation radiation and the solid angle sampled by the detection system. The pressure in the cell was therefore held in the range 20–22 Torr, and was monitored with a capacitance manometer.

The collection optics axis was separated from the fluorescence cell with an MgF_2 window, and was flushed with dry nitrogen to eliminate absorption of the light by O_2 or water vapour. The fluorescence was collected with two MgF_2 plano-convex lenses (focal length 58 mm at 180 nm, Crystran Ltd.) and focussed onto the photocathode of a photon counting module (MP921P, Perkin Elmer), which encompasses a channel photomultiplier (CPM), high voltage supply and amplifier/(factory set) discriminator/counting electronics. The module was powered by a regular laboratory power supply unit at 5 V. The CPM was set to count for 1 second time periods. Typical dark count levels were of the order of 1 s^{-1}.

2.3 Data acquisition

The signal collected at the CPM was recorded (in counts per second) continuously, and sent to a portable PC via the RS232 port. A USB-based DAQ module (USB-1208LS, Measurement Computing) was used to log auxiliary data every second, including cell pressure, lamp pressure, and microwave power. The flows through all the mass flow controllers were also logged. Various system temperatures (below) were monitored via thermocouples (type K) and a USB-based 8-channel thermocouple input module. A program to display and log all data was developed using the Delphi programming language. The instrument was housed in an enclosed lightweight aluminium frame (approximately 80×80×120 cm), and the instrument was powered from a regular 13 A extension cable.

3 Calibration

Fluorescence detection is not an absolute technique and the instrument therefore requires calibration in order to relate the signal observed to a quantity of atoms or molecules present. This is achieved by sampling known concentrations of I_2 or I and measuring the corresponding signal. The calibration setup, shown in Fig. 2, consists of a quartz flow-tube, gas supplies and mass flow controllers, and a mercury pen-ray lamp (LSP035, LOT Oriel). A fraction of the flow through the calibration tube was sampled into the RF cell, with the excess balance directed to an ozone analyser (during calibration) and vented.

3.1 Sensitivity to I_2

To calibrate the response of the instrument to I_2 fluorescence, the signal is monitored upon addition of different amounts of I_2 in a nitrogen bath gas to the calibration flow-tube. A controlled flow of nitrogen gas (10–50 sccm) was passed through a Pyrex U-tube packed alternately with I_2 crystals (>99.5%, Aldrich) and glass beads in order to completely saturate the gas with I_2 vapour. The tube was held in a water bath which acts as a thermal reservoir maintaining a stable temperature, and thus sustaining a constant vapour pressure from the I_2 crystals. The temperature of the trap was monitored with a thermocouple (type K) and recorded using the USB-based thermocouple input module. The I_2/N_2 gas mixture was diluted in a larger flow of N_2 (10 slm) at the trap exit, and sent to the flow tube. The concentration of I_2 in the flow tube may be determined using the vapour pressure of the I_2 crystals at the recorded temperature (Antoine equation parameters taken from Stull 1947),

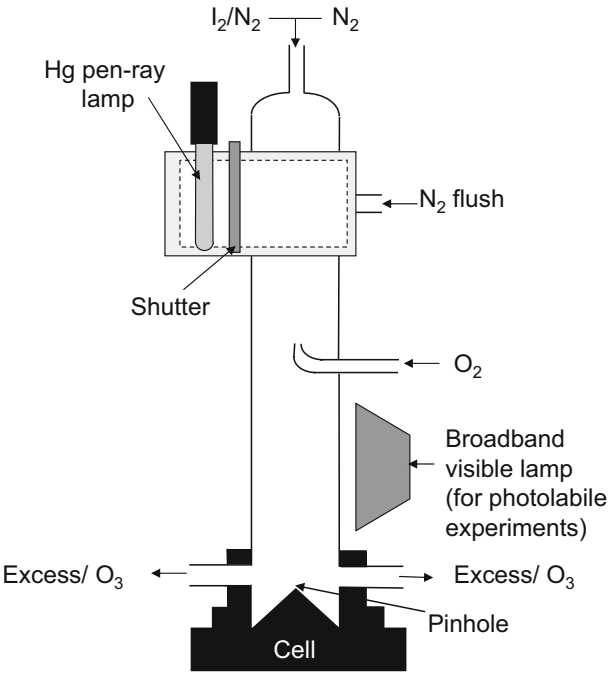

Fig. 2 Schematic diagram of the calibration/photolysis flow tube

verified by UV absorption in a separate cell. I_2 concentrations used in the calibration were in the range $3–30\times10^{12}$ molecule cm^{-3}. A plot of I_2 signal as a function of $[I_2]$ can be seen in Fig. 3. During the field deployment the sensitivity to I_2, C_{I2}, was $(8\pm0.8)\times10^{-11}$ count s^{-1} molecule^{-1} cm^3.

3.2 Sensitivity to I atoms

The sensitivity of the instrument to atomic iodine was determined by photolysing I_2 to generate known concentrations of atomic iodine. A mercury pen-ray lamp is used to photolyse I_2 at 185 nm and 254 nm ($\sigma_{185\ nm}=1.93\times10^{-17}$ cm^2 per molecule;

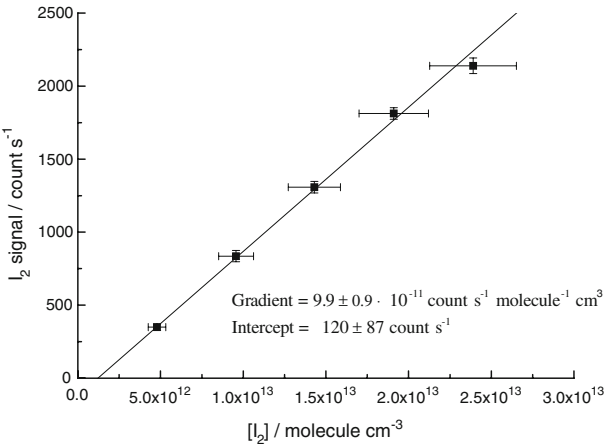

Fig. 3 Calibration plot showing measured I_2 fluorescence signal as a function of $[I_2]$ sampled from the calibration tube. The instrument sensitivity towards I_2 is equal to the gradient of the line. *y*-Axis error bars are given as the standard deviation of the I_2 fluorescence signal; *x*-axis error bars are given as the error on the determined concentration. The regression line fit is weighted to errors on both axes

$\sigma_{254\ nm}=1.13\times10^{-18}$ cm^2 per molecule; Saiz-Lopez et al. 2004); a quartz flow tube was used rather than Pyrex to allow transmission of the 185 nm light.

The pen-ray lamp was housed in an aluminium holder at a fixed distance from the fluorescence cell. The lamp was allowed to warm up to give a stable output, and was flushed with dry N_2 to keep the lamp and housing at a stable temperature and prevent absorption of the 185 nm radiation by the oxygen in air. A shutter was mounted in front of the pen-ray lamp to allow modulation of the light output/photolysis of I_2 without switching the lamp on and off. The background scattered signal was initially recorded; then, I_2 was introduced into the calibration tube and the I_2 fluorescence signal recorded. The shutter was then opened to expose the I_2 flow to the pen-ray output, generating I atoms, and giving rise to a further increase in the observed signal. The concentration of iodine atoms generated in the calibration tube could be altered by changing the current supplied to the mercury pen-ray lamp, which in turn varies the flux of the lamp (unlike molecular oxygen, the cross section of I_2 in this region is relatively smooth hence insensitive to small shifts in the lamp emission spectrum with current).

In order to determine the concentration of iodine atoms generated by photolysis of I_2, the flux from the pen-ray lamp at different applied currents must be known. The product of the lamp output flux at the wavelengths in question (F) and the exposure time for which the calibration flow was within the illuminated region (t) was determined using an ozone actinometry method similar to that described by Whalley et al. (2007): measurement of the ozone produced from photolysis of varying strength mixtures of N_2O in air, flowed through the calibration tube. The lamp flux was calibrated under the same flow conditions as were used for subsequent RF system calibrations, thus the exposure time was equivalent in both instances.

N_2O was photolysed in the presence of O_2 to generate ozone:

$$N_2O+h\nu \rightarrow O(^1D)+N_2 \tag{3}$$

$$O(^1D)+M \rightarrow O(^3P)+M \tag{4}$$

$$O(^3P)+O_2+M \rightarrow O_3+M \tag{5}$$

Some ozone will also be generated via photolysis of molecular oxygen at 185 nm:

$$O_2+h\nu \rightarrow O+O \tag{6}$$

Gas from the flow tube was sent *via* the excess lines (Fig. 2) to a commercial ozone analyzer (Thermo Electron, TE49C or 2B Technologies, Model 205), with which $[O_3]$ was monitored as the flow of N_2O was varied between 0–50 sccm. This procedure was repeated as a function of (measured) lamp current.

The product Ft may be calculated by

$$Ft=\frac{[O_3]_{measured}}{[N_2O]\sigma_{N_2O}}. \tag{7}$$

A plot of $[O_3]$ as a function of $[N_2O]$ for a range of lamp currents between 0 and 1500 μA can be seen in Fig. 4; the product Ft can be calculated from the gradient divided

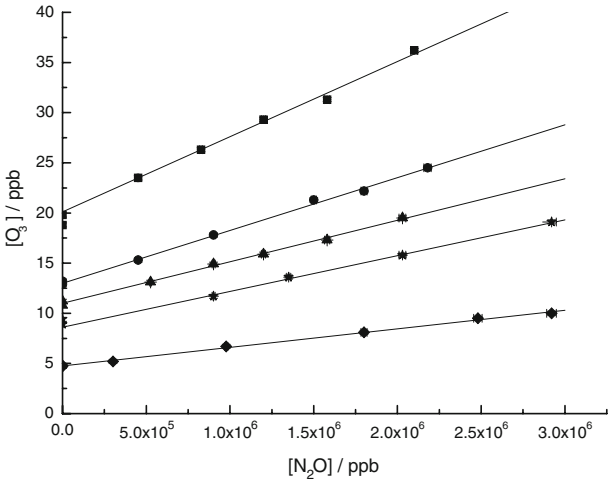

Fig. 4 Determination of the 184.9 nm photolysis flux from the mercury pen-ray lamp at various supplied lamp currents using an actinometric method (Eq. 7). Plot shows $[O_3]$ measured in the excess line as a function of $[N_2O]$ in the calibration tube. A linear regression which takes into account errors in both *x*- and *y*-axes was applied to the data. *Symbols* represent different lamp currents (μA): *square*=1,800; *circle*=1,267; *triangle*=1,010; *star*=790; *diamond*=454. Error bars are shown (but may be unclear because of their small magnitude) *y*-axis error bars represent uncertainty in the O_3 measurement; *x*-axis error bars represent uncertainty in the flows and hence concentration of N_2O. The intercepts arise from the formation of ozone from the photolysis of O_2

by the absorption cross-section of N_2O at 185 nm ($\sigma_{185\ nm}=1.43\times10^{-19}$ cm^2 per molecule). The absorption of N_2O at 254 is not significant ($\sigma_{254\ nm}<1\times10^{-23}$ cm^2 per molecule; Atkinson et al. 2004), and therefore this method determines only the flux of the 185 nm line from the lamp. The product *Ft* may then be plotted as a function of lamp current (see Fig. 5) to obtain a linear relationship between lamp current and lamp flux. The uncertainty associated with measurement of the 184.9 nm lamp flux is minimal, approximately 3%, as the uncertainties in $[N_2O]$ and σ_{N_2O} are small.

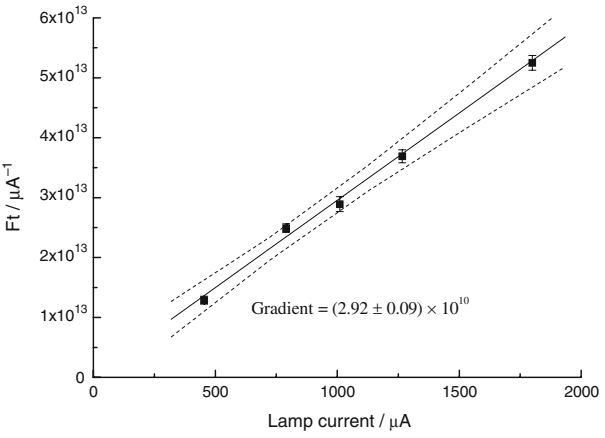

Fig. 5 Relationship between lamp photolysis flux and lamp current, derived from Fig. 4. The gradient of the line can be used to determine the lamp flux for a given lamp current. The *y*-error bars represent the uncertainty in the gradients shown in Fig. 4. *Dashed lines* indicate the 95% confidence limit on the linear regression

Once the flux emitted from the lamp is known, the concentration of iodine atoms formed upon photolysis of I_2 can be calculated via

$$[\mathrm{I}]=\left([\mathrm{I_2}]\times Ft\times\sigma_{(\mathrm{I_2}\,185)}\times 2\right)+\left([\mathrm{I_2}]\times Ft\times\sigma_{(\mathrm{I_2}\,254)}\times 2\times 15\right) \tag{8}$$

where Ft is the product of the mercury lamp flux and the exposure time (at a given lamp current) and $\sigma_{(I_2185)}$ and $\sigma_{(I_2254)}$ are the absorption cross sections of I_2 at 185 nm and 254 nm respectively. It is assumed that the quantum yield for photolysis of I_2 is 2, which is consistent with quantum yield measurements below 340 nm (Atkinson et al. 2007). The factor of 15 accounts for the intensity of the 254 nm mercury line relative to that at 185 nm (Lide 2007). The ratio of I_2 photolysed at 254 nm compared with that at 185 nm is 0.9:1.

The calibration factor for iodine atom detection, (C_I in units of count s^{-1} $atom^{-1}$ cm^3) may then be determined using

$$C_I=\frac{S_\mathrm{I}}{[\mathrm{I}]} \tag{9}$$

where S_I, the signal due to iodine atom resonance fluorescence, is given by

$$S_\mathrm{I}=S_\mathrm{total}-S_\mathrm{I2}-S_\mathrm{b} \tag{10}$$

and [I] is determined as given in Eq. 7; S_{Total} is the signal when I_2 is present and the shutter to the lamp is open, S_{I2} is the signal from I_2 fluorescence only and S_b is the background signal [comprising dark counts (typically <1 count s^{-1}), scattered light from the cell walls, air and aerosol, and any interference from other species]. Typically, five repeat points were measured at varying lamp currents and the calibration factor, C_I, is determined from the gradient of a plot of S_I vs. [I].

The iodine atom calibrations were conducted in air, to best represent atmospheric conditions. However, is was not possible to use air as the bath gas in the flow tube, as any O_2 passing in front of the mercury pen-ray lamp would be photolysed at 185 nm; the resulting O atoms and ozone would react with both I_2 and I causing an interference in the calibration method. Instead, N_2 was used as the bath gas for the I_2 in the photolysis region, and O_2 was added subsequently, through a separate injection port in the flow tube located after the photolysis region. The O_2 flow was set to make up 21% (2.1 slm) of the total flow in the calibration tube with the remainder made up from N_2 (7.9 slm). Experiments conducted in a bath gas of air showed a significant (approximately 30%) decrease in iodine atom sensitivity compared with experiments in nitrogen only, primarily as a result of the absorption of the excitation and fluorescence radiation by O_2.

The calibration conditions employed (I_2 concentration and photolysis flux, and hence I atom concentrations) were necessarily limited by the sensitivity of the detection techniques available to determine the molecular iodine concentration (UV absorption spectroscopy) and the lamp flux (ozone actinometry—ozone monitored using a commercial UV-absorption monitor); consequently calibrations were performed at levels higher than the ambient concentrations of iodine atoms and molecular iodine encountered. To verify that the instrument response was constant and linear, and to ensure that quenching of the excited I atoms or absorption of the emitted fluorescence were not appreciably enhanced by the presence of I_2, calibrations were performed over as wide a range of I_2 levels and photolysis flux values as the methodology and iodine vapour pressure would permit (see Fig. 6). These calibrations showed no significant change in sensitivity towards I atoms with [I_2] varied over the range $2–20\times10^{12}$ molecule cm^{-3}. Note that the error bars in the points shown in Fig. 6 arise from imprecision in the calibration factors (x-axis: I_2 concentration, lamp flux,

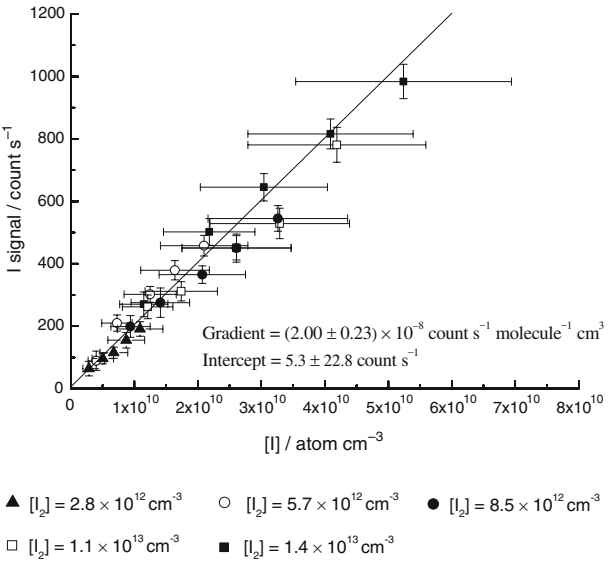

Fig. 6 Typical calibration plot showing I atom fluorescence signal as a function of [I] sampled from the calibration tube. The gradient of the line determines the instrument sensitivity towards I atoms. Symbols indicate calibration runs performed with various concentrations of I_2 in the flow tube. *y*-Axis error bars indicate the standard deviation of the I atom fluorescence signal; *x*-axis error bars indicate the uncertainty in the calculated concentration of [I], arising from the lamp flux measurement and the I_2 concentration determination. The regression line takes into account errors on both the *x*- and *y*-axes

flow rates) and the fluorescence signal (*y*-axis, including contribution from subtraction of I_2 fluorescence signal); the latter factor in particular is much larger under the calibration conditions than is the case in ambient air. The uncertainty in the regresson line parameters reflects the fact that Fig. 6 is a composite of five separate calibration runs performed at different times with different I_2 concentrations, indicating the invariance of the instrument response. The uncertainty in the gradient of Fig. 6, 11.5%, is factored into the overall uncertainty in the reported I atom measurements.

The effect of water vapour on the sensitivity of the instrument was also investigated. The O_2 gas injected into the side arm was first bubbled through a trap containing water in order to saturate the gas; again it was necessary to inject the water vapour after the photolysis region to avoid any interference in the iodine chemistry from HO_x radicals formed by water photolysis. H_2O vapour was varied in the range 0–1.4% which is comparable to levels found in ambient air (during the measurements at Mace Head, reported below, the mean relative humidity was 88%, corresponding to a water vapour fraction of 1.4%). The instrument sensitivity was found to be constant (within uncertainty) over this range.

The Reynolds number which describes the flow in the calibration tube is calculated to be 650 at a total flow of 10 slm (in a tube of internal diameter 2.1 cm at a pressure of 760 Torr and a temperature of 298 K), and hence the flow is within the laminar regime. Under these conditions the axial velocity will be greatest at the centre of the calibration tube. In similar experimental arrangements (Aschmutat et al. 1994) this effect has been shown to lead to lower radical concentrations at the centre of the flow tube relative to the periphery (as the gas in the centre of the tube is exposed to the photolysis light for a shorter time). Because the lamp flux is measured by sampling ozone from the excess line (at the edge of the tube) this could lead to an overestimation of the lamp flux, and thus an underestimation of the calibration factor. A correction for this effect can be applied and may be termed the gas profile factor, *P*, equal to the ratio of the ozone concentration in the central region of the tube, drawn into the RF cell, to that in the excess flow measured by the ozone analyser.

However, tests to measure $[O_3]$ at the centre of the calibration tube compared with at the edge of the tube, confirmed that in our experimental setup, P=1; the injection of O_2 from the side arm introduces sufficient turbulence to thoroughly mix the flow, effectively eliminating the concentration gradient. A consequence of this is that some wall-loss of iodine atoms, in the turbulence induced by the O_2 addition, may occur, implying a potential underestimation of the system sensitivity—see below. During the field deployment at Mace Head, short calibrations were performed daily to monitor any significant change in the sensitivity of the instrument, with full calibrations as described above (data shown in Fig. 6) conducted in Leeds. The calibration factor during the field measurements was $C_I=(2.0\pm 0.4)\times 10^{-8}$ count s^{-1} $atom^{-1}$ cm^3.

3.3 Uncertainties and limit of detection

A breakdown of the uncertainties associated with both the I_2 and I atom sensitivity is shown in Table 1. The limit of detection for measurement systems recording small numbers of discrete events (such as photon counting of fluorescence measurements) may be calculated using Eqs. 11 and 12 (Stevens et al. 1994):

$$\mathrm{LOD} = \frac{\mathrm{S/N}}{C_{(\mathrm{I_2\ or\ I})}}\sqrt{\left(\frac{1}{m}+\frac{1}{n}\right)}\sigma_\mathrm{b} \tag{11}$$

where S/N is the signal to noise ratio (in this case, S/N=1), C is the pertinent calibration factor (in count s^{-1} $molecule^{-1}$/$atom^{-1}$ cm^3) for I_2 or I accordingly, m is the number of data acquisition points taken when measuring the I_2 or I signal and n is the number of data points taken when measuring the background (usually m=n=30 or 60) and σ_b is the standard deviation of the background data points given by

$$\sigma_\mathrm{b} = \sqrt{\frac{1}{t}S_\mathrm{b}} \tag{12}$$

where t is the time period for the acquisition of a single data point in seconds (usually 1 s) and S_b is the background signal (count s^{-1}).

For I_2, the limit of detection was typically around 1.3 ppb (using $C_{I2}=8\times 10^{-11}$ count s^{-1} $molecule^{-1}$ cm^3, S/N=1, m=n=60, t=1 and a typical value for S_b of 200 count s^{-1}). For iodine atoms, the limit of detection was typically 5.3 ppt (using $C_I=2\times 10^{-8}$ count s^{-1} $molecule^{-1}$ cm^3, and similar values of S/N, m, n, t and S_b). The limit of detection can be decreased if m and n are increased, but there will be a trade off between a lower limit of detection and a low temporal resolution.

Table 1 Breakdown of the uncertainties associated with both the I_2 and I atom sensitivity

Parameter	$\pm 1\sigma$ uncertainty (%)
$[O_3]$	1
$[N_2O]$	1
Ft	3
$[I_2]$	11
C_{I2}	10
C_I	10

4 Modes of operation

The instrument can be operated in two different modes; either to measure ambient iodine atoms, or to measure the total photolabile iodine loading, through broadband visible photolysis of ambient air, with detection of the iodine atoms released. Direct detection of I_2 at larger concentrations (several orders of magnitude larger than ambient levels), for example, as emitted directly from seaweeds in an enclosed chamber (see Section 5.1), as well as indirect detection by photolysis with a broadband light source and subsequent detection of the iodine atoms formed, may also be accomplished.

4.1 Measurement of ambient iodine atoms

When run in ambient sampling mode, air is drawn into the fluorescence cell via the pinhole, and iodine atoms detected as described earlier. During the field deployment, it was found necessary to attach a short length (approximately 1 cm) of blackened Teflon tube over the pinhole in order to block solar radiation from entering the cell, which would otherwise obscure the fluorescence signal (since the CPM is not blind to the extreme lower wavelengths of solar radiation in the troposphere). The Teflon tubing was sealed onto the pinhole with a small piece of neoprene. Subsequent tests showed that this sampling tube did not alter the sensitivity of the instrument to iodine atoms within the uncertainty of the calibration.

Contributions to the signal detected at the CPM arise not only from fluorescence of iodine atoms present in the cell, but also from any dark current on the CPM, scattered light from the cell walls and from aerosol, and potential chemical interferences from other species, including I_2. In order to obtain the signal from fluorescence of iodine atoms only, this background signal must be subtracted from the total signal recorded, and can only be measured once the iodine atoms have been removed from the sampled air. Ambient air is alternately sampled either directly into the detection cell or is first passed through a darkened pre-reactor, within which iodine atoms are removed through their reaction with ambient ozone:

$$I + O_3 \rightarrow IO + O_2 \tag{13}$$

The darkened pre-reactor was fabricated from a blacked-out Pyrex tube (diameter 50 mm; length 70 cm) with a 90° curve midway, blocked at one end and with a hole to sample via a short length of 6 mm tubing into the fluorescence cell. The lifetime of I atoms with respect to reaction with ambient O_3 is approximately 1.1 s, calculated using $k_{(12)}= 1.2\times10^{-12}$ cm^3 molecule^{-1} s^{-1} at 288 K (Atkinson et al. 2007) and using the average O_3 of 30.2 ppb observed during the field deployment. The residence time in the darkened reactor was calculated to be approximately 14 s, in which period almost all (>99.99%) the iodine atoms will be removed through reaction with ambient O_3. Sampling between the ambient sampling tube and the darkened reactor was modulated manually every 60 s. The modulation between direct sampling and darkened pre-reactor therefore allows subtraction of any contribution to the RF signal from other fluorescing species (including I_2) and aerosol scatter.

4.2 Measurement of photolabile iodine species

The alternative configuration of the instrument is to measure the total concentration of photolabile iodine-containing species, by employing a broadband visible halogen lamp

to photolyse ambient air, followed by detection of any iodine atoms so formed. In this configuration, air was passed through the calibration tube, within which photolysis took place, before entering the RF cell. Ambient air was sampled through 6 mm OD PTFE tubing into the calibration flow tube which was mounted over the pinhole in the usual manner. A small pump was attached via a mass flow controller to the excess gas lines to draw air through the PTFE tubing and flow tube at a total flow rate of 7 slm (comprising 5.4 slm through the pinhole and 1.6 slm through the excess line). The broadband lamp was mounted at the bottom of the flow tube, approximately 3 cm above the pinhole and detection cell. The lamp was modulated on/off (details below), and any iodine atoms released from photolysis of iodine-containing species in the ambient air were detected in the usual manner after sampling through the pinhole into the fluorescence cell, with the background signal measured when the photolysis lamp was off. The photolysis lamp also significantly heated the flow tube, raising concern over the potential for thermal dissociation of iodine-containing particles (e.g. nascent I_xO_y aerosol). To avoid complications from this effect, the temperature of the tube was monitored with a thermocouple, and the lamp was switched off when the temperature reached 40°C (usually after about 5 s). The tube was then allowed to cool to below 27°C before the next photolysis period, a period of 20–30 s. The background signal was taken as an average of 25 data points when the lamp was off and the temperature was between 20°C and 35°C; the measurement signal was taken as the average of 5 data points when the lamp was on and the temperature was between 20°C and 40°C. We do not anticipate any significant thermolysis of iodine-containing species over this temperature range, in the <0.2 s transit time from the warmed region to the RF cell entrance—considering the most likely candidate for thermal decomposition, iodine nitrate, only 1% would decompose at 40°C in this time (decomposition rate from Allan and Plane 2002)—although very little is known concerning the thermal stability of higher iodine oxides.

The total photolabile iodine loading may be represented qualitatively as the iodine atoms released after photolysis of all iodine-containing species, with a relative sensitivity to different species given by the products of their absorption cross sections, I atom photolysis quantum yields, and the emission spectrum of the photolysis lamp. It is likely, at least at the Mace Head site of the field deployment, that the major contributor to iodine atoms from broadband visible photolysis lamp would be I_2, since I_2 has the largest absorption cross section of the known inorganic iodine species, in the visible wavelength region (Saiz-Lopez et al. 2004), and comparison of previous observations of I_2 and iodocarbons at Mace Head (Saiz-Lopez and Plane 2004; Carpenter et al. 1999) indicate that level of molecular iodine is much greater (by nearly two orders of magnitude) than the sum of the measured organic iodine species. The sensitivity of the total photolabile iodine measurement to molecular iodine was obtained by measuring the iodine atom signal resulting from photolysis of a known concentration of I_2 in air, using the broadband photolysis lamp:

$$C_{\mathrm{PL,I_2}} = \frac{S_{\mathrm{PL}}}{[\mathrm{I_2}]} \tag{14}$$

where $C_{\mathrm{PL,I2}}$ is the calibration factor for the photolysis lamp, S_{PL} is the iodine atom signal measured with the photolysis lamp turned on (after subtraction of background, including I_2 fluorescence) in the presence of a known concentration of I_2. Figure 7 shows the variation in S_{PL} with $[I_2]$; the gradient of this graph determines the sensitivity of the

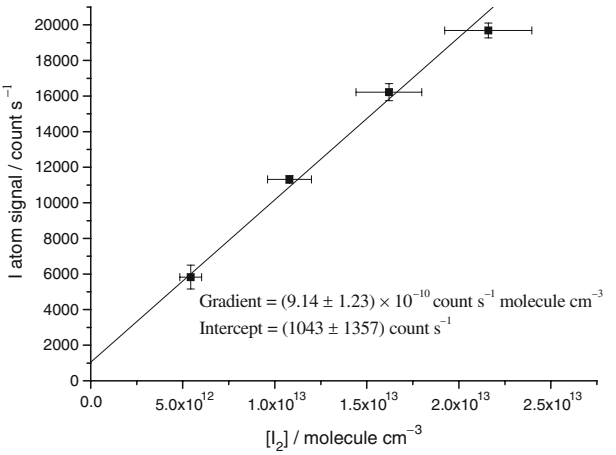

Fig. 7 Relationship between iodine atom signal and I_2 concentration, in the photolabile configuration (I_2 photolysis within the calibration tube, by the broadband photolysis lamp); the gradient of the line determines $C_{I2,PL}$ (eq. 14). *y*-Axis error bars represent the standard deviation of the fluorescence signal; *x*-axis error bars represent the uncertainty in the I_2 concentration. The linear regression takes into account both *x*- and *y*-errors

photolabile iodine measurement (to molecular iodine), $C_{PL,I2}=(9.1\pm1.2)\times10^{-10}$ counts s^{-1} molecule^{-1} cm^3. Note that $C_{PL,I2}$ implicitly incorporates the quantum yield for I atom production from I_2 photolysis. Equation 14 may then be applied to the measured iodine signal from ambient air, in the photolabile measurement configuration, to yield the concentration of I_2 present, under the assumption that I_2 is the species which dominates this signal.

In a laboratory setting, molecular iodine can also be detected through its direct fluorescence without the need for prior photolytic conversion to iodine atoms, but the sensitivity (C_{I2}, 8×10^{-11} counts s^{-1} molecule^{-1} cm^3) is approximately an order of magnitude worse that that obtained through I atom detection following photolysis, insufficient for atmospheric measurements. Comparison of the sensitivity of the photolabile measurement with that for iodine atoms yields the photolysis efficiency for I_2:

$$\text{Photolysis efficiency} = \frac{C_{PL,I_2}}{2 \times C_I} \tag{15}$$

where the factor of 2 accounts for the iodine atom quantum yield. Application of Eq. 15 to the relevant calibration factors determines an I_2 photolysis efficiency of 2.3%.

5 Mace head field measurements

The instrument was deployed for the first time in the field in August 2007 at the Mace Head Atmospheric Research Station on the west coast of Ireland (53° N, 9° W). This location is well known for boundary layer halogen activity (e.g. Alicke et al. 1999; Carpenter et al. 2000; Allan et al. 2000); a description of the site and prevailing chemical and meteorological conditions during summer is given by Heard et al. (2006). Measurements in the iodine atom configuration were performed just to the north of the shore-side laboratory building, at a position with open access to airflow from the ocean, at an elevation of approximately 5 m above mean sea level. In the photolabile iodine configuration, the instrument was located within the shoreline laboratories, and ambient air was sampled on the western (ocean) side from approximately 2 m above ground level.

5.1 Emission of molecular iodine from seaweed

Whilst on site at Mace Head, the instrument was used to observe direct emission of I_2 from seaweed. Small amounts of six different species of seaweed, including *Himanthalia elongata*, *Palmaria palmata*, and *Laminaria digitata* were gathered from rock pools exposed during one of the lowest tides.

Synthetic air was flowed through a large Pyrex flask (volume=2 l) and into the calibration tube at a rate of 10 slm. After the background signal had been recorded, 50 g of the (wet) seaweed sample was added to the Pyrex vessel. The broadband visible lamp was used to photolyse any I_2 (and any other photolabile species present) in the calibration tube for about 5 seconds at approximately one minute intervals. Only one type of seaweed was observed to emit detectable levels of I_2: *Laminaria digitata*.

As shown in Fig. 8, 50 g of *Laminaria digitata* was observed to emit I_2 at levels of up to 300 ppb, which decreased over the period of about an hour. Agitation of the seaweed in the vessel released a further burst of I_2. These high levels were observed without intentionally stressing the seaweed; no O_3 was present since the bath gas used was (cylinder) compressed air, and the actinic intensity (indoors, within the Pyrex vessel) was moderate. The seaweed was kept in seawater until tested (within 30 minutes of harvesting), and was not dried before testing, although the sample gradually dried out over time due to the flow through the vessel. The leaves of the seaweed were not deliberately damaged or cut. Palmer et al. (2005) suggested that under oxidative stress (caused by either exogenous hydrogen peroxide, gaseous ozone or a solution of oligoguluronates, known elicitors of oxidative stress) the seaweed *Laminaria digitata* increased production of I_2. Therefore, levels of I_2 emitted from this type of seaweed under atmospheric conditions could be significantly greater than those reported here.

In the seaweed experiment, I_2 concentrations were obtained both indirectly, via photolysis and subsequent detection of the iodine atoms released, and by directly observing the (much weaker) I_2 fluorescence. The excellent agreement between the two determinations of $[I_2]$ apparent from the plot (Fig. 8) gives confidence in the calibration methods used.

5.2 Measurement of ambient iodine atoms

Iodine atoms were observed during the day of the 29 August 2007. For these measurements, the instrument was located about 45 m from the high-tide water line, and

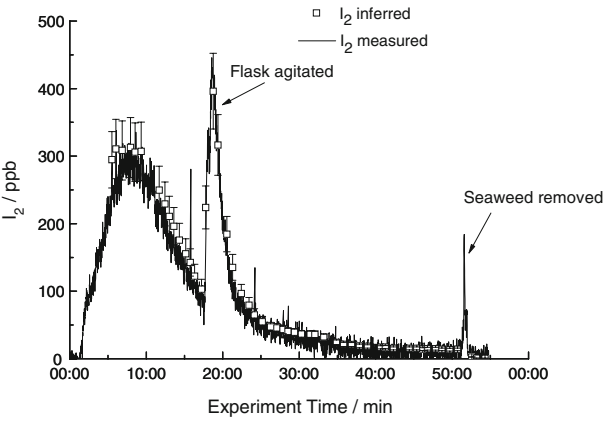

Fig. 8 Time series showing levels of I_2 emitted directly from a 10 slm flow of synthetic air over a 50 g sample of *Laminaria digitata* seaweed within a 2 l flask.. The *black line* represents $[I_2]$ measured directly. The *open squares* represent $[I_2]$ inferred after photolysis with the broadband visible lamp and detection of the iodine atoms formed; the *y*-axis errors are given by the uncertainty in the gradient of Fig. 7

approximately 100 m from the low-tide line. Figure 9 presents a plot showing the time series for iodine atoms; the measurements are well above the limit of detection (calculated from the measured calibration factor and the background signal) of the instrument, which was around 3 ppt for a 300 s integration period. The peak in iodine atoms correlates strongly with the local low tide (data recorded at Roundstone Bay; Admiralty Easytide database; August 2007), which supports the hypothesis of a local coastal source of I_2 and/or the alkyl iodide precursors. It is interesting to note that the rock pools containing *Laminaria digitata*, which we have shown directly emits I_2, and other seaweeds of a similar type (e.g. *Laminaria saccharina*) were only exposed at the very lowest tides experienced at Mace Head, as was the case on 29 August. On inspection of the data recorded at a temporal resolution of 1 s, it was apparent that the iodine atom concentrations are highly variable, and fluctuate greatly on this timescale (relative standard deviation of 300%), implying a highly variable atmospheric iodine flux. Given the close proximity to the exposed pools containing seaweed known to emit I_2 (approximately 50–100 m), and the short lifetime of molecular iodine with respect to photolysis (5–10 s when the sun is overhead; Saiz-Lopez et al. 2004), any variation in the wind speed and direction will greatly affect the processing time and hence the concentration of atomic iodine.

The concentrations reported here may be overestimates of the levels of atomic iodine sampled for two reasons: If a significant proportion of aerosol particles were lost to the walls of the darkened reactor, then the background signal measurement might appear lower than during the ambient measurement period, when the increased aerosol would add to the light scattering and increase the apparent fluorescence signal. Secondly, if significant levels of iodine atoms were lost during calibration, as a consequence of wall encounters during turbulence introduced by the O_2 addition, the calibration constant (C_I) would be reduced, and the retrieved ambient iodine atom levels overestimated, although we believe this to be a minor effect. Developments are in progress to address these issues (improving the various flow geometries). The values presented may therefore represent upper limits on the levels of atomic iodine present.

5.3 Measurement of photolabile species

Experiments to measure the total photolabile iodine content of ambient air were carried out during several night-time and day-time periods throughout the Mace Head campaign. At

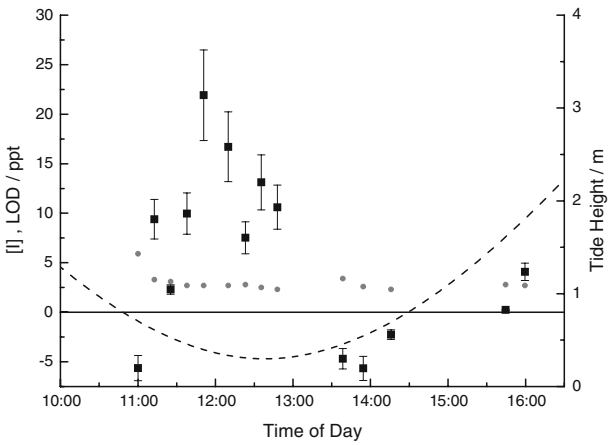

Fig. 9 Time series (local time IST) showing ambient I atoms (5 min integration period) at Mace Head on 29 Aug 2007. The *grey circles* represent the limit of detection for a 5 min integration period. The *dashed line* represents the tide height

night-time, in particular, it is likely that the majority of the photolabile iodine will be released from molecular iodine, and levels of I_2 will build up in the absence of solar photolysis. Figure 10 shows a plot of inferred I_2 mixing ratio (calculated using Eq. 14) as a function of tide height during the night of the 16/17 August 2007. It is apparent that the levels of I_2 are higher at low tide, which is in agreement with the hypothesis that seaweed species such as *Laminaria digitata* emit high levels of I_2 directly when exposed—an equivalent plot of measured I_2 as a function of tidal height using observations made during the NAMBLEX campaign by Saiz-Lopez et al. (2006) shows a strikingly similar trend over the same tidal height range.

5.4 Comparison with previous observations

Gas-phase reactive inorganic iodine species (IO, I_2) have been observed at Mace Head previously using long-path differential optical absorption spectroscopy (LP-DOAS) techniques, which determine average mixing levels along a 4–8 km lightpath (Alicke et al. 1999; Allan et al. 2000; Saiz-Lopez and Plane 2004), while in situ measurements of I_2 have been performed at Mace Head using cavity ring-down spectroscopy (CRDS; Bitter et al. 2005), and at nearby locations using denuder tubes coupled with ICP/MS analysis (Siaz-Lopez et al. 2006). The LP-DOAS observations of IO have ranged from <1 to 7 ppt, with I_2 observed at up to 93 ppt (night) and 20 ppt (day). The in situ observations have detected I_2 at up to 94 ppt (CRDS) and 115 ppt (denuder samples), supporting the conclusion from the observations reported here, that local littoral sources dominate the inorganic iodine activity at Mace Head. Saiz-Lopez et al. (2006) have modelled the inorganic iodine chemistry anticipated for different iodine source distributions, ranging from an even distribution along the DOAS beampath through to solely local shoreline emissions, constraining their model scenarios with the LP-DOAS, CRDS and denuder observations. In the shoreline sources only case, they predict daytime levels of I_2, IO and I atoms of 80–100, 40–50 and 15–20 ppt respectively, in good qualitative agreement with the observations reported here. Most recently, Commane et al. (2008) have reported new in situ measurements of IO radicals by laser-induced fluorescence, performed at Mace Head during August 2008; the observations (up to 34 ppt IO, correlated with tide height) are consistent with the I atom and photolabile

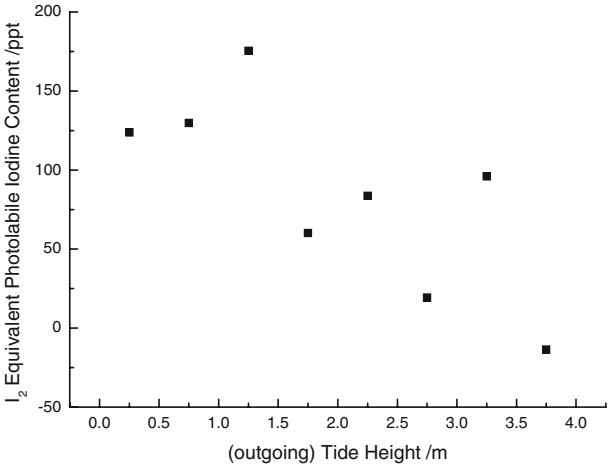

Fig. 10 Photoproduced iodine atom signal, depicted as I_2 mixing-ratio equivalent, after photolysis of ambient air, as a function of tide height at Mace Head during the night of 16/17 Aug 2007 (20:30–03:00 local time)

iodine measurements reported in this work, and with the overall inorganic iodine distribution simulated by Saiz-Lopez et al. (2006), for the shoreline sources only case.

6 Summary

A portable field instrument employing resonance fluorescence has been developed and has been shown to be sufficiently sensitive for the selective measurement of ambient levels of atomic iodine. The limit of detection achieved with this instrument, 5.3 ppt, is significantly lower than has been reached previously in systems for laboratory-based kinetics/photochemistry experiments. Observations made at the Mace Head Atmospheric Research Station in August 2007 indicate that iodine atoms are present at levels up to 22±5 ppt at low tide. This measurement represents the first direct observation of iodine atoms in the marine boundary layer. The instrument has also been used to measure the total photolabile iodine loading of ambient air, at Mace Head probably corresponding predominantly to I_2, and hence to infer the I_2 abundance; observations overnight determined molecular iodine levels of up to 200 ppt. Future modifications to the instrument will improve the sensitivity of the photolabile detection technique, including the addition of a selective photolysis capability. With some further development, the instrument could be used in a variety of measurement modes, for example on ship or aircraft platforms.

Acknowledgements The authors would like to thank the staff at the Mace Head Atmospheric Research Station and NUI Galway, in particular G. Jennings and G. Spain. Meteorological and supporting measurements were provided by G. Spain. Thanks also to colleagues at the University of Leeds; in particular A. Goddard, J. Dixon and P. Halford-Maw for technical assistance and advice. Support for access to Mace Head was given by the European Community—Research Infrastructure Action under EUSAAR TNA programme. The funding for this research was provided by the UK Natural Environment Research Council (grant NE/D005272/1).

References

Admiralty Easytide database. http://easytide.ukho.gov.uk/EasyTide/EasyTide/index.aspx. Cited August 2007

Alicke, B., Hebestreit, K., Stutz, J., Platt, U.: Iodine oxide in the marine boundary layer. Nature. **397**, 572–573 (1999). doi:10.1038/17508

Allan, B.J., Plane, J.M.C.: A study of the recombination of IO with NO_2 and the stability of INO_3: implications for the atmospheric chemistry of iodine. J. Phys. Chem. A. **106**, 8634–8641 (2002). doi:10.1021/jp020089q

Allan, B.J., McFiggans, G., Plane, J.M.C., Coe, H.: Observations of iodine monoxide in the remote marine boundary layer. J. Geophys. Res. **105**(Dll), 14363–14369 (2000)

Anderson, J.G., Margitan, J.J., Stedman, D.H.: Atomic chlorine and the chlorine monoxide radical in the stratosphere: three in situ observations. Science **198**, 501–503 (1977). doi:10.1126/science.198.4316.501

Anderson, J.G., Grassl, H.J., Shetter, R.E., Margitan, J.J.: Stratospheric free chlorine measured by balloon-borne in situ resonance fluorescence. J. Geophys. Res. **85**(C5), 2869–2887 (1980). doi:10.1029/JC085iC05p02869

Aschmutat, U., Hessling, M., Holland, F., Hofzumahaus, A.: A tunable source of hydroxyl (OH) and hydroperoxy (HO_2) radicals: in the range between 10^6 and 10^9 cm^{-3}, *Physico-Chemical Behaviour of Atmospheric Pollutants*, G. Angeletti and C. Restelli, Eds., Proc. EUR 15609, 811–816 (1994)

Atkinson, R.L., Baulch, D.L., Cox, R.A., Crowley, J.N., Hampson, R.F., Hynes, R.G., et al.: Evaluated kinetic and photochemical data for atmospheric chemistry: volume I—gas phase reactions of O_x, HO_x, NO_x and SO_x species. Atmos. Chem. Phys. **4**, 1461–1738 (2004)

Atkinson, R.L., Baulch, D.L., Cox, R.A., Crowley, J.N., Hampson, R.F., Hynes, R.G., et al.: Evaluated kinetic and photochemical data for atmospheric chemistry: volume III—gas phase reactions of inorganic halogens. Atmos. Chem. Phys. **7**, 981–1191 (2007)

Bitter, M., Ball, S.M., Povey, I.M., Jones, R.L.: A broadband cavity ringdown spectrometer for in-situ measurements of atmospheric trace gases. Atmos. Chem. Phys. **5**, 2547–2560 (2005)

Bloss, W.J., Lee, J.D., Johnson, G.P., Sommariva, R., Heard, D.E., Saiz-Lopez, A., et al.: Impact of halogen monoxide chemistry upon boundary layer OH and HO_2 concentrations at a coastal site. Geophys. Res. Lett. **32**, L06814 (2005). doi:10.1029/2004GL022084

Brewer, L., Tellinghuisen, J.B.: Detection of iodine atoms by an atomic fluorescence technique: application to study of diffusion and wall recombination. J. Chem. Phys. **54**(12), 5133–5138 (1971). doi:10.1063/1.1674807

Brune, W.H., Weinstock, E.M., Anderson, J.G.: Midlatitude chlorine oxide below 22 km altitude: measurements with a new aircraft-borne instrument. Geophys. Res. Lett **15**(2), 144–147 (1988). doi:10.1029/GL015i002p00144

Brune, W.H., Anderson, J.G., Chan, K.R.: In situ observations of ClO in the Antarctic: ER-2 aircraft results from 54°S to 72°S latitude. J. Geophys. Res. **94**(D14), 16649–16663 (1989a). doi:10.1029/JD094iD14p16649

Brune, W.H., Anderson, J.G., Chan, K.R.: In situ observations of BrO over Antarctica: ER-2 aircraft results from 54°S to 72°S latitude. J. Geophys. Res. **94**(D14), 16639–16647 (1989b). doi:10.1029/JD094iD14p16639

Carpenter, L.J.: Iodine in the marine boundary layer. Chem. Rev. **103**, 4953–4962 (2003). doi:10.1021/cr0206465

Carpenter, L.J., Sturges, W.T., Penkett, S.A., Liss, P.S., Alicke, B., Hebestreit, K., et al.: Short-lived alkyl iodides and bromides at Mace Head, Ireland: links to biogenic sources and halogen oxide production. J. Geophys. Res. **104**(D1), 1679–1689 (1999). doi:10.1029/98JD02746

Carpenter, L.J., Malin, G., Liss, P.S., Küpper, F.C.: Novel biogenic iodine-containing trihalomethanes and other short-lived halocarbons in the coastal East Atlantic. Glob Biogeochem. Cycles. **14**(4), 1191–1204 (2000). doi:10.1029/2000GB001257

Chameides, W.L., Davis, D.D.: Iodine—its possible role in tropospheric photochemistry. J. Geophys. Res. **85**, 7383–7398 (1980). doi:10.1029/JC085iC12p07383

Commane, R., Bale, C.S.E., Furneaux, K.L., Ingham, T., Whalley, L.K., Heard, D.E.: Heard, Bloss, W.: Impacts of iodine monoxide in the marine boundary layer. Geophys. Res. Abstr. 10, EGU2008-A-04243 (2008)

Gross, U., Ubelis, A., Spietz, P., Burrows, J.: Iodine and mercury resonance lamps for kinetics experiments and their spectra in the far ultraviolet. J. Phys. D Appl. Phys. **33**, 1588–1591 (2000). doi:10.1088/0022-3727/33/13/305

Heard, D.E., Read, K.A., Methven, J., Al-Haider, S., Bloss, W.J., Johnson, G.P., et al.: The North Atlantic Marine Boundary Layer Experiment (NAMBLEX). Overview of the campaign held at Mace Head, Ireland, in summer 2002. Atmos. Chem. Phys. **6**, 2241–2272 (2006)

Ingham, T., Cameron, M., Crowley, J.N.: Photodissociation of IO (355 nm) and OIO (532 nm): quantum yields for $O(^3P)$ and $I(^2P_J)$ production. J. Phys. Chem. A. **104**, 8001–8010 (2000). doi:10.1021/jp001166p

Lide, D.R. (ed.): CRC handbook of chemistry and physics, Internet Version 2007, 87th edn. Taylor and Francis, Boca Raton, FL (2007). http://www.hbcpnetbase.com

O'Dowd, C.D., Hoffmann, T.: Coastal new particle formation: a review of the current state-of-the-art. Environ. Chem. **2**, 245–255 (2005). doi:10.1071/EN05077

O'Dowd, C.D., Jimenez, J.L., Bahreini, R., Flagan, R.C., Seinfeld, J.H., Hämeri, K., et al.: Marine aerosol formation from biogenic iodine emissions. Nature. **417**, 632–636 (2002). doi:10.1038/nature00775

O'Grady, B.V., Lain, L., Donovan, R.J., Gower, M.C.: Competition between reactive and inelastic processes involving I_2 ($D^1\sigma_u^+$). Chem. Phys. Lett. **91**(6), 491–493 (1982). doi:10.1016/0009-2614(82)83097-2

Palmer, C.J., Anders, T.L., Carpenter, L.J., Küpper, F.C., McFiggans, G.G.: Iodine and halocarbon response of *Laminaria digitata* to oxidative stress and links to atmospheric new particle production. Environ. Chem. **2**, 282–290 (2005). doi:10.1071/EN05078

Peters, C., Pechtl, S., Stutz, J., Hebstreit, K., Hönninger, G., Heumann, K.G., et al.: Reactive and organic halogen species in three different European coastal environments. Atmos. Chem. Phys. **5**, 3357–3375 (2005)

Plane, J.M.C., Husain, D.: Measurement of the absolute third-order rate constant for the reaction between K+I+He by time-resolved atomic resonance fluorescence monitoring of iodine atoms in the vacuum ultraviolet ($I(5p^46s(^2P_{3/2}))$–$I(5p5(^2P^0_{3/2}))$) coupled with steady atomic fluorescence on atomic potassium ($K5^2P_J$) –$K(4^2S_{1/2})$). J. Phys. Chem. **90**, 501–507 (1986). doi:10.1021/j100275a030

Platt, U., Hönninger, G.: The role of halogen species in the troposphere. Chemosphere. **52**, 325–338 (2003). doi:10.1016/S0045-6535(03)00216-9

Saiz-Lopez, A., Plane, J.M.C.: Novel iodine chemistry in the marine boundary layer. Geophys. Res. Lett **31**, L04112.1–L04412.4 (2004). doi:10.1029/2003GL019215

Saiz-Lopez, A., Saunders, R.W., Joseph, D.M., Ashworth, S.H., Plane, J.M.C.: Absolute absorption cross-section and photolysis rate of I_2. Atmos. Chem. Phys. **4**, 1443–1450 (2004)

Saiz-Lopez, A., Shillito, J.A., Coe, H., Plane, J.M.C.: Measurements and modelling of I_2, IO, OIO, BrO and NO_3 in the mid-latitude marine boundary layer. Atmos. Chem. Phys. **6**, 1513–1528 (2006)

Saiz-Lopez, A., Mahajan, A.S., Salmon, R.A., Bauguitte, S.J.-B., Jones, A.E., Roscoe, H.K., et al.: Boundary layer halogens in coastal Antarctica. Science. **317**, 348–351 (2007). doi:10.1126/science.1141408

Solomon, S., Garcia, R.R., Ravishankara, A.R.: On the role of iodine in ozone depletion. J. Geophys. Res. **99** (D10), 20491–20499 (1994). doi:10.1029/94JD02028

Stevens, P.S., Mather, J.H., Brune, W.H.: Measurement of tropospheric OH and HO_2 by laser-induced fluorescence at low pressure. J. Geophys. Res. **99**(D2), 3543–3557 (1994). doi:10.1029/93JD03342

Stimpfle, R.M., Wilmouth, D.M., Salawitch, R.J., Anderson, J.G.: First measurements of ClOOCl in the stratosphere: the coupling of ClOOCl and ClO in the Arctic polar vortex. J. Geophys. Res. **109**, D03301 (2004). doi:10.1029/2003JD003811

Stull, D.R.: Vapor pressure of pure substances organic compounds. Ind. Eng. Chem. **39**, 517–540 (1947). doi:10.1021/ie50448a022

Vogt, R., Sander, R., Von Glasow, R., Crutzen, P.J.: Iodine chemistry and its role in halogen activation and ozone loss in the marine boundary layer: a model study. J. Atmos. Chem. **32**, 375–395 (1999). doi:10.1023/A:1006179901037

von Glasow, R., Crutzen, P.J.: Tropospheric halogen chemistry. In: Holland, H.D., Turekian, K. K. (eds.) Treatise on Geochemistry, vol. 4(02), pp. 1–67. Elsevier, Amsterdam (2007)

Von Hobe, M., Grooß, J.-U., Müller, R., Hrechanyy, S., Winkler, U., Stroh, F.: A re-evaluation of the ClO/Cl_2O_2 equilibrium constant based on stratospheric in-situ observations. Atmos. Chem. Phys. **5**, 693–702 (2005)

Von Hobe, M., Ulanovsky, A., Volk, C.M., Grooß, J.-U., Tilmes, S., Konopka, P., et al.: Severe ozone depletion in the cold Arctic winter 2004–05. Geophys. Res. Lett. **33**, L17815 (2006). doi:10.1029/2006GL026945

Whalley, L.K., Furneaux, K.L., Gravestock, T., Atkinson, H.M., Bale, C.S.E., Ingham, T., et al.: Detection of iodine monoxide radicals in the marine boundary layer using laser induced fluorescence spectroscopy. J. Atmos. Chem. **58**, 19–39 (2007). doi:10.1007/s10874-007-9075-9